AAS 23-311

JETTISON AND DISPOSAL FROM NEAR RECTILINEAR HALO ORBITS, PART 1: THEORY

Stephen T. Scheuerle,[*] Diane C. Davis,[†] Emily M. Zimovan-Spreen,[‡] Brian P. McCarthy,[§] Damennick B. Henry[**], and Kathleen C. Howell[††]

The proposed Gateway spacecraft in a Near Rectilinear Halo Orbit (NRHO) will be a human outpost in cislunar space. The baseline mission may experience the deployment of visiting vehicles, cubesats, and on-orbit debris. Departure from the NRHO and cislunar space is nontrivial due to the complex gravitational environment that persists in and around Gateway. Long-term disposal orbits in heliocentric space offer safe destinations for deployed objects. To mitigate risks associated with conjunctions between Gateway and deployed objects, strategies to identify risk-avoidant paths to heliocentric space are necessary for Gateway mission operations.

INTRODUCTION

Knowledge of the dynamical regime is crucial for successful cislunar mission operations. One facet of mission design considers on-orbit object or debris jettison. Jettisoned material from a spacecraft may aid the primary mission in reducing vehicle mass, deploying scientific experiments (such as cubesats), or end-of-life disposal. Proper jettison procedures are essential to avoid collisions, satisfy planetary protection constraints, and minimize the accumulation of space debris, which can pose significant risks to future missions and the Gateway itself. The demand for a strategy is amplified due to the challenges faced by cislunar debris tracking capabilities. The aim of this investigation is to identify the procedures necessary to properly dispose of or jettison objects from cislunar space.

The guiding motivation behind this analysis is to generate strategies for the proposed Gateway crew outpost. The baseline orbit for Gateway is an L_2 southern Near Rectilinear Halo Orbit (NRHO) with a 9:2 resonance with the Earth-Moon-Sun synodic period. The orbit relies on the gravitational forces of the Earth and Moon to complete each revolution, as it is a periodic solution in the Earth-Moon Circular Restricted Three-body Problem (CR3BP). As Gateway will operate in cislunar space, jettisoned objects will be exposed to the same complex regime as the outpost. Identifying disposal strategies is necessary to mitigate collision risks. A characteristic of the Earth-Moon system is that with proper departure conditions, deployed objects escape to heliocentric space along ballistic arcs. To preserve heritage sites on the lunar surface and avoid passage near the Earth, heliocentric escape offers a long-term debris mitigation strategy if both short- and long-term trajectory behavior is carefully considered. A key challenge in accomplishing heliocentric escape is effectively leveraging the Sun-Earth and Earth-Moon dynamics. The aim of this investigation is to introduce a

[*] Ph.D. Candidate, Purdue University, 701 W. Stadium Ave, West Lafayette, IN 47907, sscheuer@purdue.edu
[†] Gateway Mission Design Lead, Flight Mechanics and Trajectory Design Branch, NASA Johnson Space Center, diane.c.davis@nasa.gov
[‡] Gateway Mission Design Engineer, Flight Mechanics and Trajectory Design Branch, NASA Johnson Space Center, emily.m.spreen@nasa.gov
[§] Gateway Mission Design Engineer, a.i. solutions, Inc., brian.p.mccarthy@nasa.gov
[**] Ph.D. Candidate, University of Colorado Boulder, damennick.henry@colorado.edu
[††] Hsu Lo Distinguished Professor, School of Aeronautics and Astronautics, Purdue University, howell@purdue.edu

jettison strategy such that with a single deterministic maneuver from the NRHO, an object departs to heliocentric space.

Previous studies introduce the idea and demand for NRHO disposal capabilities. Olikara et al. explore long-term heliocentric disposal from Sun-Earth libration point orbits. Strategies include utilizing manifold structures off Lyapunov and Halo orbits to reach heliocentric space, and the cost associated with a cleanup maneuver to avoid future returns to the Earth.[1] Further analysis by Colombo et al. in 2014 explore several mission end-of-life strategies for spacecraft in Sun-Earth libration point orbits, one option being a heliocentric disposal strategy.[2] In 2015, Whitley and Martinez explore possible staging orbit options in cislunar space to enable future missions to the surface of the Moon. The analysis presents the NRHO as an orbital outpost option for upcoming crewed cislunar program, later named Gateway and the Artemis program.[3] In 2017, Williams et al. investigate long-term mission capabilities for an operational crewed outpost in an Earth-Moon NRHO. The study contains a preliminary look into the disposal dynamics from the NRHO. The analysis presents seven disposal types: interior, exterior, Moon-crossing, near-Moon, Earth impact, Moon impact, and heliocentric escape. Of the seven disposal types, three are defined to be 'permanent options', heliocentric escape, Earth-impact, and Moon-impact.[4] To both maintain the NRHO structure, and identify motion departing the orbit, a metric that indicates an object is escaping the orbit is necessary. Guzzetti et al. introduce a modified momentum integral to signal motion departing from a NRHO.[5]

Risk-avoidant escape to heliocentric space from the Earth-Moon NRHO requires the culmination of several stages of flight. The demand to identify operational strategies in the NRHO grew as the orbit became the baseline for the Gateway program. In 2018, Boudad et al. presents NRHO disposal strategies that employ the Bicircular Restricted Four-body Problem (BCR4BP). The strategies apply energy-like metrics, solar tidal effects, and mapping techniques to illuminate trends in departing flow from the Earth-Moon system. The analysis also includes cases that impact the Earth and Moon prior to heliocentric escape.[6] In 2019, Davis et al. explore the capabilities of NRHO disposal for both lunar impact and escape to heliocentric space. The strategy considers the time to depart the NRHO and tidal influence of the Sun. To avoid potential conjunction hazards, a strategy to mark safe maneuvers directions from Gateway is introduced. Given the name 'recontact map', the purpose of the tool is to illustrate maneuver directions that could pose a threat for future conjunctions.[7] The construction of recontact maps requires computational resources; Phillips et al. explore the potential for cloud computing in the NRHO to construct such maps.[8] A Hamiltonian map is introduced by Davis et al. to illustrate transfer options with sufficient energy to reach heliocentric space. The analysis also explores strategies for disposal through lunar impact.[9] In 2021, Guardabasso et al. inspect the probability of various disposal strategies for jettison maneuvers along the velocity and anti-velocity directions.[10] One challenge that persists is the dimensionality of the problem. With the ability to change maneuver direction, magnitude, and location along the orbit, classifying trends is nontrivial. Thus, for the lunar impact study, Davis et al. apply three-dimensional maps to illustrate the repeating, cyclic pattern in maneuver behavior. The work explores the probability of lunar impact at varying maneuver magnitudes and directions.[11] In 2022, Davis et al. combine insights from the dynamics and a sensitivity analysis through the Cauchy-Green strain tensor to characterize 'green zones' for Cubesat deployment from the NRHO. The analysis compares Cubesat range information with respect to the linear stretching principal directions and defines a flip geometry in range plots.[12] There is extensive analysis into the different phases and types of disposal strategies from the NRHO. As the object departs to heliocentric space, the problem focuses on avoiding returns to the Earth-Moon system. Analysis into the stability of different orbital resonances and maps aids in classifying the dominating the dynamics. Anderson et al. explore the orbital resonance structures in the Jupiter-Europa system to a quarantine region in the vicinity of the Galilean moons. The methodology considers several Poincaré maps to characterize stable islands.[13] Understanding the proper methods to combine the phases of the disposal into one end-to-end transfer is crucial to providing long-term, risk-adverse paths to heliocentric space.

JETTISON STRATEGY

Characteristics that govern passage through the Earth-Moon and Sun-Earth dynamical regimes offer insight into identifying cislunar disposal strategies. The jettisoned object is assumed to follow a ballistic path after the initial maneuver away from the reference spacecraft. Therefore, recognizing how properties of the transfer evolve over time offers insight into the long-term disposal problem. The main objective is to mitigate conjunction or impact events between the jettisoned object and other spacecraft, the Earth, or the Moon.

Thus, the strategy aims to identify the ideal jettison maneuver direction for a given location on the NRHO, maneuver size, and epoch. The jettison strategy introduced in this investigation is separated into three phases. The phases are NRHO departure, heliocentric escape, and Earth evasion. Previous work explores each of these phases independently, but the aim is to combine each strategy to create one end-to-end method. A jettison is treated as an impulsive maneuver starting from a state along the 9:2 NRHO. An overview of the three separate phases is as follows:

1. Departure from the NRHO is the first disposal phase. Due to the linear stability properties of the 9:2 NRHO being characterized as slightly unstable, a small perturbation from the orbit causes objects to asymptotically depart over time. The time to depart from the NRHO is a function of the jettison location along the NRHO, maneuver magnitude, and maneuver direction. Zimovan-Spreen et al. identify that Gateway departs from the NRHO between 45 and 72 days if no orbit maintenance maneuvers are performed.[14] A small jettison maneuver from Gateway causes an object to depart over several months. However, during this timeframe, the jettisoned object may pass close to Gateway on future revolutions of the orbit. During this timeframe, it is necessary to determine whether a conjunction between Gateway and the jettisoned object will arise. A sample trajectory of that departs the 9:2 NRHO is illustrated in Figure 1. The jettison maneuver is 2 m/s at an osculating true anomaly (TA) of 200°. The trajectory is modeled in the CR3BP, where the arrows indicate the direction of motion along the blue arc. The aim for the NRHO departure phase is to identify jettison directions that avoid possible conjunction events.

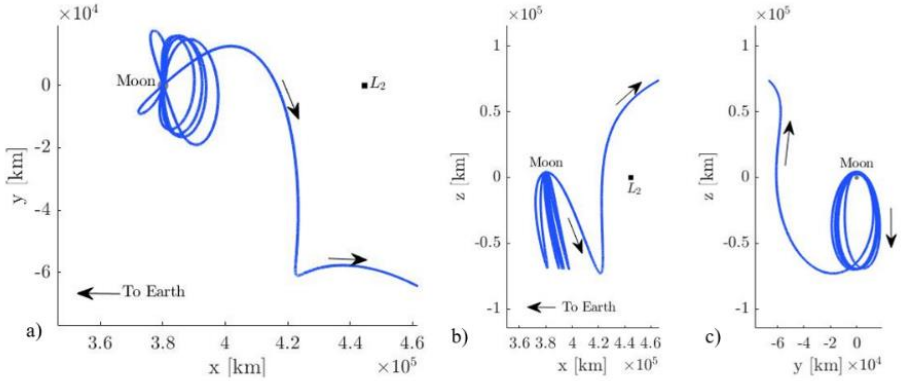

Figure 1: Example of the NRHO Disposal phase in the Earth-Moon rotating frame (modeled in the CR3BP): a) xy-projection, b) xz-projection, c) yz-projection

2. The heliocentric escape phase aims to ensure the deployed object escapes from the Earth-Moon vicinity. After NRHO departure, an object may remain near the Moon, travel toward Earth interior to the Moon, or depart exterior to the Moon, away from the Earth. A transfer that remains in the vicinity of the Earth-Moon system may encounter lunar passes that influence the long-term behavior of the trajectory or may risk conjunction with other spacecraft or the Earth itself. Thus, to avoid impacting the Earth, Moon, or other spacecraft, exterior departures in the Earth-Moon system are desired. The heliocentric escape phase begins once the object is exterior to Moon in the Earth-Moon system (> 450,000 km from Earth) and ends when the object leaves the Earth's sphere of influence. The energy of the spacecraft at the start of the heliocentric escape phase, as well as the orientation of the Earth-Moon-Sun system at NRHO departure, govern patterns in escaping to heliocentric space. A sample trajectory that successfully escapes to heliocentric space is illustrated in Figure 2. The blue trajectory departs from the NRHO and voyages through the L_1 portal toward heliocentric space. The transfer is modeled in the BCR4BP and depicted in the Sun-B_1 rotating frame, centered at the Earth-Moon barycenter (B_1). The trajectory in Figure 2 is the continuation of the NRHO disposal transfer from Figure 1. The investigation aims to achieve direct escapes, i.e., transfers that escape without additional revolutions within the Earth-Moon system. Such access to heliocentric space is a function of the energy of the object post-lunar departure and the influence of solar perturbations, i.e., relative orientation of the Sun.

3. Long-term Earth evasion is the goal of the third phase of disposal. Sun-Earth resonant structures offer insight into long-term passes of the disposed object and Earth. The motion of the escaping object is primarily governed by the Sun once it departs from the Earth (greater than three million km from Earth). However, over 50 to 100 years, the slight differences in orbital period between the object and Earth lead to approaches on regular intervals (every 10-20 years). Although the close approach is certain, the distance varies as a function of the phase and orbital resonance of the deployed object. A sample departure transfer is illustrated in Figure 3. The trajectory is modeled in the BCR4BP and depicted in the Sun-centered, Sun-B_1 rotating frame. The path is propagated for 16-years and is the continuation of the transfers illustrated in Figure 1 and Figure 2. The Earth evasion phase aims to identify strategies that enable long term disposal strategies that avoid returns that traverse near the Earth.

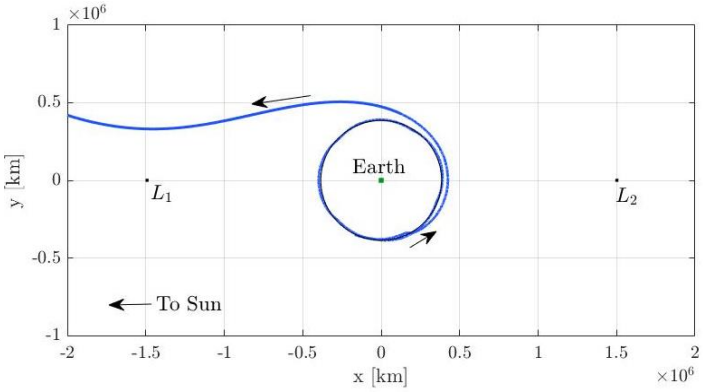

Figure 2: Heliocentric escape trajectory in the Sun-B_1 rotating frame, centered at B_1 (modeled in the BCR4BP)

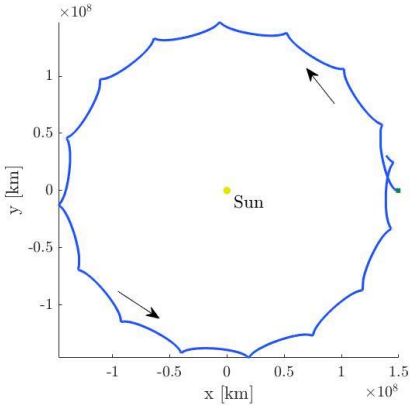

Figure 3: Sample Earth evasion transfer in the Sun-B_1 rotating frame

DYNAMICAL MODELS

The Circular Restricted Three-body Problem (CR3BP) and the Bicircular Restricted Four-body Problem (BCR4BP) model the motion of jettisoned objects in this investigation. The Earth-Moon CR3BP models the motion of an object during the NRHO departure phase. Beyond 450,000 km from Earth, the BCR4BP becomes the underlying dynamical model. Once the object departs the Earth-Moon system, the Sun-Earth CR3BP is applied. The implementation of the four-body problem aids in describing solar perturbations near the Earth-Moon system.

The CR3BP is a paramount in constructing initial guesses and identifying patterns for complex trajectory design in a multi-body regime. Consider three bodies defined as P_1, P_2, and P_3, with masses M_1, M_2, and M_3, respectively. Each body is assumed to be a point mass. In this study, P_1 is the Earth, P_2 is the Moon, and P_3 is spacecraft. The CR3BP relies on a set of simplifying assumptions that reduce the complexity of the three-body problem. Assume the mass of the spacecraft is negligible compared to the other two celestial bodies, i.e., $M_3 \ll M_1, M_2$ such that the motion of P_1 and P_2 is independent of the spacecraft. Also assume that the Earth and Moon traverse in circular orbits about their mutual barycenter (B_1). A rotating coordinate frame is considered, where the origin is the barycenter B_1, and the primaries P_1 and P_2 lie on the *x*-axis. To aid in numerical methods, the system is nondimensionalized such that the distance between the Earth and Moon is equal to one, and the sidereal period of the Earth-Moon system is 2π. The position of the primary bodies is a function of the mass parameter μ, computed as $\mu = \frac{M_2}{M_1+M_2}$. The position of the Earth is at (-μ , 0 ,0), while the Moon resides at (1- μ ,0 ,0). The governing equations of motion of the spacecraft are second order, coupled, nonlinear differential equations. Formulating the equations relative to a reference frame rotates with the larger primary bodies (Earth and Moon) yields the following time-independent equations,

$$\ddot{x} = 2\dot{y} + x - \frac{(1-\mu)(x+\mu)}{r_{13}^3} - \frac{\mu(x-1+\mu)}{r_{23}^3}$$

$$\ddot{y} = -2\dot{x} + y - \frac{(1-\mu)y}{r_{13}^3} - \frac{\mu y}{r_{23}^3}$$

$$\ddot{z} = -\frac{(1-\mu)z}{r_{13}^3} - \frac{\mu z}{r_{23}^3} \quad (1)$$

The quantities r_{ij} are the scalar radial distance from primary P_i to P_j. The terms $(\dot{x}, \dot{y}, \dot{z})$ and $(\ddot{x}, \ddot{y}, \ddot{z})$ are the velocity and acceleration terms in the rotating frame, respectively.

As the object leaves the immediate vicinity of the Moon, gravity perturbations from the Sun increase. Therefore, the Earth-Moon-Sun BCR4BP is applied. The BCR4BP follows similar assumptions to the CR3BP, where the model describes the motion of a spacecraft about the gravitational influence of a star-planet-moon system. The Earth and Moon follow circular orbits about their mutual barycenter (B_1), and the Sun and B_1 traverse in circular orbits about the mutual barycenter (B_2). The Earth-Moon and Sun-B_1 orbital planes are assumed to be coplanar. Unlike in the CR3BP, the equations of motion for the BCR4BP cannot be written in terms of a time-independent system. However, the model is periodic with the synodic period of the Earth-Moon-Sun system. The position of the Sun relative is

$$\vec{r}_4 = [a_S cos(\theta_S) \quad a_S \sin(\theta_S) \quad 0] \quad (2)$$

where a_S is the scalar distance between the Sun and Earth-Moon barycenter, and θ_S is called the Sun angle, that orients the Sun in the Earth-Moon rotating frame. The angular rate of the Sun equals the difference between the mean motion of the Sun-B_1 system and the Earth-Moon system, i.e., $\dot{\theta}_S = n_{SB_1}$- 1 for a system that is nondimensionalized by the Earth-Moon orbital period. The equations of motion are

$$\begin{aligned}
\ddot{x} &= 2\dot{y} + x - \frac{(1-\mu)(x+\mu)}{r_{13}^3} - \frac{\mu(x-1+\mu)}{r_{23}^3} - \frac{m_s(x - a_S\cos(\theta_S))}{r_{43}^3} - \frac{m_s\cos(\theta_S)}{a_S^2} \\
\ddot{y} &= -2\dot{x} + y - \frac{(1-\mu)y}{r_{13}^3} - \frac{\mu y}{r_{23}^3} - \frac{m_s(y - a_S\sin(\theta_S))}{r_{43}^3} - \frac{m_s\sin(\theta_S)}{a_S^2} \\
\ddot{z} &= -\frac{(1-\mu)z}{r_{13}^3} - \frac{\mu z}{r_{23}^3} - \frac{m_s z}{r_{43}^3}
\end{aligned} \quad (3)$$

The term m_s is the mass of the Sun relative to the Earth-Moon system, i.e. , $m_s = \frac{M_4}{M_1+M_2}$. For the Earth-Moon-Sun system the relative mass of the Sun is $m_s \approx 328900$. It is often advantageous to view trajectories in the BCR4BP within both the Earth-Moon and Sun-B_1 rotating frame to recognize patterns.

Energy-like quantities offer insight into accessible regions of space and disposal strategies. The CR3BP has an integral of the motion denoted the Jacobi Constant value. The Jacobi Constant (JC) is expressed as,

$$JC = -(\dot{x} + \dot{y} + \dot{z})^2 + (x^2 + y^2) + 2\left(\frac{1-\mu}{r_{13}} + \frac{\mu}{r_{23}}\right) \quad (4)$$

The Jacobi Constant provides an energy-like metric as a basis of comparison between trajectories. The Jacobi Constant inversely related to the energy of the object, i.e., an increase in the Jacobi Constant corresponds to a reduction in energy. A similar quantity exists in the BCR4BP, denoted the Earth-Moon Hamiltonian. Unlike the Jacobi Constant, the Hamiltonian is not an integral of the motion, due to the explicit time dependency in the equations of motion. However, much like the Jacobi Constant, the Hamiltonian acts as a metric of comparing the energy between transfer geometries, as well as the capability to traverse through the Earth-Moon-Sun system. The Hamiltonian is defined as,

$$H = -(\dot{x} + \dot{y} + \dot{z})^2 + (x^2 + y^2) + 2\left(\frac{1-\mu}{r_{13}} + \frac{\mu}{r_{23}} + \frac{m_s}{r_{43}} - \frac{m_s}{a_s}(xcos(\theta_S) + ysin(\theta_S))\right) \quad (5)$$

Previous work connects the variation in the Earth-Moon Hamiltonian with the position of the spacecraft in the Sun-B_1 rotating frame.[15] The Jacobi Constant and Hamiltonian values govern zero velocity surfaces. The zero velocity surfaces enable passage through the Earth-Moon and Sun-B_1 rotating frames.[16] The energy-like quantities offer valuable insight into the disposal structures to heliocentric space.

MANEUVER FRAME

Describing the jettison direction in a maneuver frame enables repeatable geometry across revolutions in the NRHO. For mission operations, defining a maneuver relative to an inertial reference frame provides clarity across subsystems. As the 9:2 NRHO is not periodic in an inertial frame, the maneuver direction changes each revolution. To provide consistency across revolutions, the maneuvers are defined relative to a Velocity, Normal, and Binormal (VNB) frame. The coordinate frame is constructed by the following unit vectors,

$$\vec{N}^I = \vec{r}_{23}^I \times \vec{V}^I$$

$$\hat{B}^I = \vec{V}^I \times \vec{N}^I$$

$$\hat{V}^I = \frac{\vec{V}^I}{|\vec{V}^I|}, \hat{N}^I = \frac{\vec{N}^I}{|\vec{N}^I|}, \hat{B}^I = \frac{\vec{B}^I}{|\vec{B}^I|}$$

where arrow overbar indicates a vector, whereas the carrot overbar is a unit vector. The superscript *I* marks the vector in a Moon-centered, inertial reference frame. The velocity, binormal, and normal unit vectors are $\hat{V}^I$, $\hat{N}^I$, and $\hat{B}^I$, respectively. The investigation defines the maneuver relative to the VNB frame with yaw (Ψ) and pitch (Θ) angles. Yaw orients the maneuver relative to the $\hat{V}^I - \hat{B}^I$ plane, while pitch inclines the maneuver out of the $\hat{V}^I - \hat{B}^I$ plane and into $\hat{N}^I$. The yaw and pitch angles are illustrated in Figure 4.

Maneuver execution maps are employed to identify valuable jettison directions. Jettison from the NRHO is often restricted by operational constraints. For a disposal that is limited by maneuver magnitude and location along the NRHO, a map is generated to associate a unique direction with a desired outcome. The map is fixed with a specific maneuver magnitude, and location along the NRHO. The map scans between 0 and 360 degrees in yaw, and -90 and 90 degrees in pitch, representing maneuvers in any direction. Two different strategies are applied to discretize points along the map. The first approach builds a grid of points the resolution of two degrees, yielding 90 rows of points (pitch), and 180 columns (yaw). The second technique applies a Fibonacci spiral distribution to distribute points (5000) across a sphere.[4,17] The grid strategy is often advantageous for visual inspection and selecting points off the map. The Fibonacci spiral more evenly distributes the points across the entire sphere, which offers insight into the probability of achieving a specified outcome. Where the grid strategy is utilized for maneuver design and operations, the Fibonacci spiral aids in identifying larger trends for mission design. The placement of points along a sphere for the grid and Fibonacci spiral are illustrated in Figure 5.

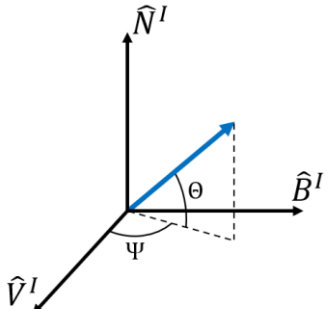

Figure 4: Yaw (Ψ) and pitch angles (Θ) in the VNB maneuver frame

NRHO DEPARTURE

The upmost priority for jettison and disposal strategies is to avoid conjunctions. The chaotic dynamics present in cislunar space, partnered with the navigation and maneuver execution errors, result in a large variance for a disposed object. Especially for debris analysis, it is unlikely the ejected material will be operational for tracking and orbit determination. Thus, modelling the precise conjunction of two objects in cislunar space is a challenge. To address the uncertainty, Davis et al. introduce the recontact analysis with Gateway.[3]

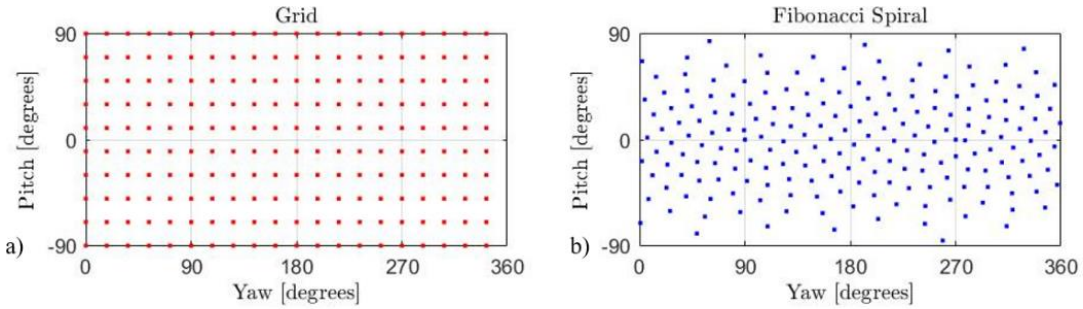

Figure 5: Points along a sphere for a grid (a) and Fibonacci spiral (b)

Recontact and range flip conditions are two conjunction events to be avoided. The investigation analyzes the risk of conjunction by recording the range between Gateway and the jettisoned object and signifying cases that approach within a set distance. Recontact is defined when a jettisoned object that departs the vicinity of Gateway returns within a keep-out sphere. The radius is assumed to be a constant, scalar value denoted the recontact distance. An object is classified as a recontact if, after jettison, it exits the keep-out sphere and subsequently reenters. Waiting until the object departs the keep-out zone ensures that recontacts are not flagged immediately after jettison. The selection of a larger recontact distance allows for a more conservative risk-mitigation strategy. In this analysis, the **recontact distance is set to 100 km**. Another conjunction hazard is denoted a range flip, or flip for short. For low energy jettison strategies, i.e., transfers explored in this analysis, the deployed object remains in the vicinity of the NRHO for several revolutions. While departing the NRHO, conjunction events near perilune are to be avoided. As the velocity peaks near perilune, the range between Gateway and the jettisoned object is subject to change rapidly. For a majority of perilune passages the range increases, however, on occasion the two objects rapidly approach each other near perilune. The name 'flip' is given to label the quick change in range. Mathematically, a **flip is defined when the range at perilune is less than the range at the previous apolune and within 1000 km**. Although the flip may not pass within the recontact distance, perturbations to the states may lead to the miss distance to shrink. Three sample range measurements are depicted in Figure 6 to demonstrate nominal, recontact, and flip patterns. The range is computed in the CR3BP by computing the distance between the jettisoned object and the position of Gateway. The motion of Gateway is assumed to follow the 9:2 synodic resonant NRHO. Each of the three arcs represent jettisons that occur at apolune with a maneuver magnitude of 1 m/s. The jettison direction is different for the three trajectories. The time along the arc is measured in units of revolutions past jettison, where one revolution is approximately 6.56 days in duration. The range axis is scaled logarithmically to illustrate general trends. The horizontal line at 100 km marks the recontact zone. Perilune passes occur at each half-integer. The red arc returns within the 100 km recontact distance near apolune approximately two revolutions after jettison. The green trajectory marks a transfer that has two flips at the first (0.5 revolution) and third (2.5 revolution) perilunes. The blue trajectory is a nominal NRHO departure: over the first three revolutions the transfer does not return within the recontact sphere nor experience a flip. Note that all three trajectories remain in the vicinity of the NRHO after the third revolution, i.e., approximately 19.5 days.

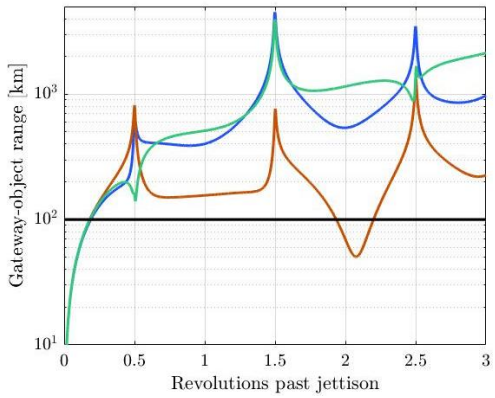

Figure 6: Three sample Gateway-object range plots computed in the CR3BP; blue, green, and red arcs are nominal, flip, and recontact cases, respectively

Recontact and flip maps aid in identifying favorable jettison directions. The range plot in Figure 6 aids in visualizing the progression of distance from Gateway over time, however, trends between maneuver direction and recontact are not easily identified from such lots. Therefore, range information from a set of disposal trajectories is projected onto a grid of points in the maneuver frame. A sample recontact map is illustrated in Figure 7. The map is generated by propagating 180 by 90 points, distributed in a grid pattern (see Figure 5). Each jettison occurs at apolune with a maneuver magnitude of 1 m/s. The range between the jettisoned object and the Gateway is assessed for a time horizon of 90 days. The yaw and pitch angles are defined relative to the VNB maneuver frame with respect to the inertial velocity. The white regions indicate locations where recontact does not occur. The colors represent the distance for solutions that recontact. For cases where multiple recontacts occur, the closest approach is selected.

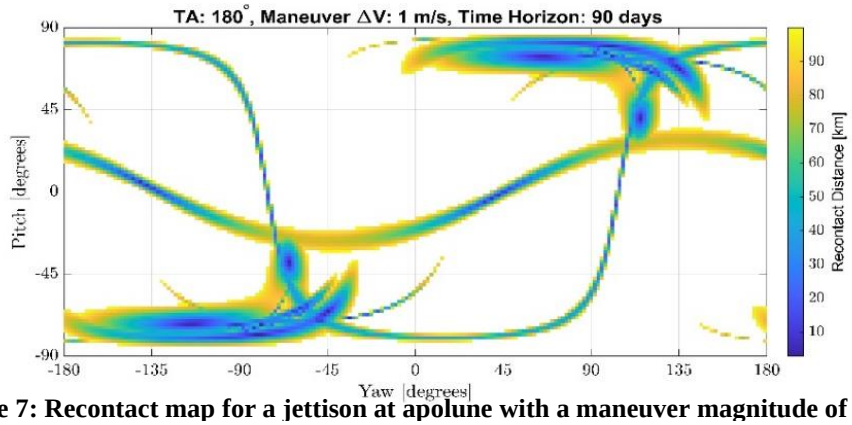

Figure 7: Recontact map for a jettison at apolune with a maneuver magnitude of 1 m/s

Recontact characteristics offer insight into risks associated with regions on the map. Taking the same sample scenario from Figure 7, three more maps are depicted in Figure 8. The map in Figure 8a demonstrates the relative velocity between the jettisoned object and Gateway during the closest approach. The number of recontacts over the horizon time is portrayed in Figure 8b, with 14 recontacts being the most occurrences over the 90-day time horizon. The location along the NRHO where recontacts occur is expressed in Figure 8c. Coloring the maps offers vast insight into the different types of recontacts. For example, examining Figure 8a and Figure 8c demonstrate that there is a higher relative recontact velocity when the recontact occurs near perilune. Likewise, comparing Figure 8b and Figure 8c highlights a relationship between recontact locations near apolune and high numbers of recontacts within a given trajectory. A range flip map appears in Figure 9 for the same sample case. Recall a flip is defined to have an approach distance within 1000 km. Thus, each point colored black in Figure 9 represents a flip departure. Note that both recontacts and flips must be avoided for an NRHO departure phase to be considered successful. Therefore, a desired NRHO departure transfer is acquired by overlaying the two maps and picking a jettison direction that avoids recontact and flips. Note that the map is dependent on the jettison maneuver magnitude and location along the NRHO. Changing one or both quantities influence the resulting maps.

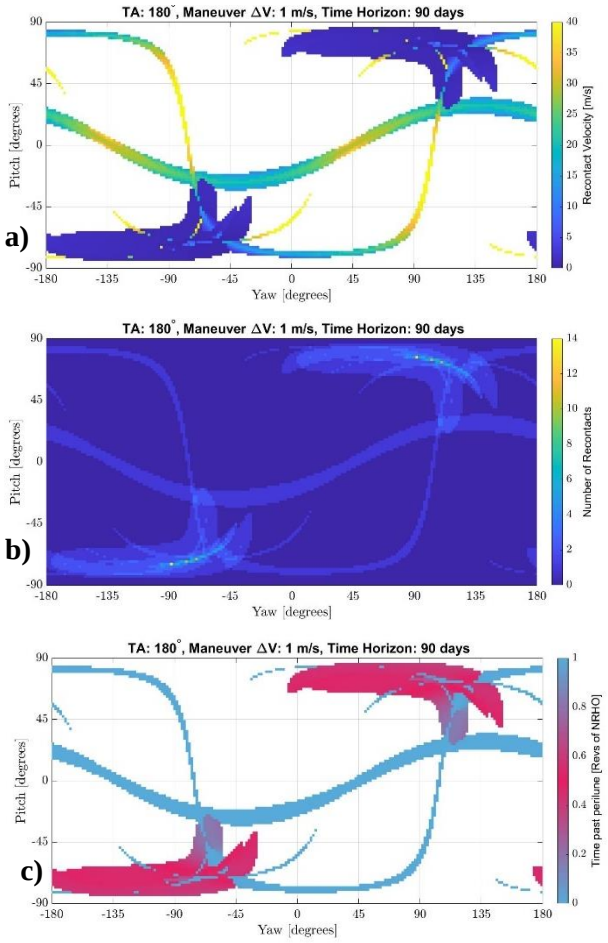

Figure 8: Recontact maps depicting the a) velocity at recontact, b) number of recontacts, and c) time past perilune for the recontact location

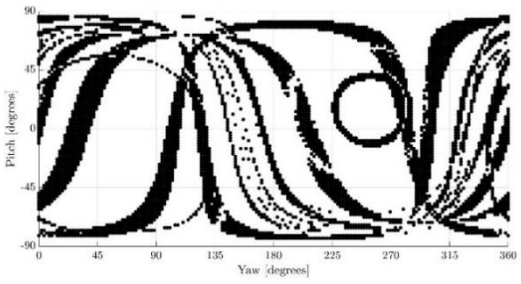

Figure 9: Range flip map generated in the CR3BP, jettison of 1 m/s at apolune

HELIOCENTRIC ESCAPE

Once the jettisoned object departs the NRHO, it may remain near the Moon, pass through the Earth-Moon L_1 portal toward Earth, or depart exterior to the Earth-Moon system through the Earth-Moon L_2 portal. To avoid impacting the Earth, Moon, or other spacecraft, exterior departures from the Earth-Moon system are desired. Access to heliocentric space is a function of the energy of the object post-lunar departure.[2] The Sun-Earth Jacobi Constant is a direct indicator of whether ballistic arcs have sufficient energy to pass through the L_1 and L_2 regimes in the Sun-Earth system. Although the energy restricts or enables access to heliocentric escape, it does not guarantee escape. The relative orientation of the Sun with respect to the Earth and Moon influences solar gravity perturbations. Past analysis noted specific conditions for desired escape for maneuvers placed at perilune.[2] The current investigation continues the analysis to evaluate the Sun-Earth Jacobi Constant value and epoch conditions to enable heliocentric escape.

Jettison geometry within cislunar space influences the Sun-Earth Jacobi Constant value attained one the object passes into heliocentric space. Recall the Jacobi Constant value is an integral of the motion for the CR3BP. For a trajectory near the Earth-Moon system, such as the NRHO and neighboring cislunar structures, the Earth-Moon Jacobi Constant value remains constant along a ballistic arc. For a transfer in heliocentric space, far from the Moon, the Sun-Earth Jacobi constant remains constant along the trajectory. However, if the Sun-Earth Jacobi constant is evaluated for a trajectory modeled in the Earth-Moon CR3BP, the value varies. This variation in the Sun-Earth Jacobi Constant ultimately enables transfers to heliocentric space. The NRHO departure phase illustrated in Figure 1 demonstrates that a jettisoned trajectory includes several passes of the Moon prior to heliocentric escape. In the Sun-Earth rotating frame, the lunar passes are equivalent to flybys that deliver or remove energy from the system. The aim is to identify NRHO departure conditions that mimic energy-increasing flybys and result in desirable energy characteristics. Previous analysis employs the use of Hamiltonian maps.[9] A similar Jacobi Constant map is generated by propagating a grid of 180 by 90 points until each transfer reaches 450,000 km from Earth. If the trajectory remains within 450,000 km from Earth for 90 days, then the jettison either remains near the Moon or departs through the Earth-Moon L_1 Gateway towards Earth; such a jettison is labeled a non-departure. Distance from Earth (rather than distance to the Moon) is designated as the departure condition to differentiate between interior and exterior paths from the lunar vicinity. Jettisons that depart from the Earth-Moon system are rotated into the Sun-Earth rotating frame, and the instantaneous Sun-Earth Jacobi Constant is determined. The current analysis assumes the intended jettison follows a direct escape, where the transfer does not have lunar flybys after the first departure from cislunar space. Recall the sample scenario described previously, in which an object is jettisoned from Gateway at apolune, with a maneuver magnitude of 1 m/s. The Jacobi Constant map for the sample scenario is illustrated in Figure 10. As the Jacobi Constant value is inversely related to an energy-like quantity, the blue regions indicate a higher energy. The areas of the map that are not colored are jettison directions that do not yield lunar departure, i.e., do not reach 450,000 km from Earth within 90 days. To reach heliocentric space from the Earth-Moon system, the trajectory must pass through the Sun-Earth L_1 or L_2 portals. A Jacobi Constant value below that of the respective Lagrange points is required. The Jacobi Constant value for Sun-Earth L_2, JC_{L_2} =3.000886, is applied as a more conservative metric. Reconsider the map depicted in Figure 10. Any point with a value greater than 3.000886 is not feasible for direct, heliocentric escape. The map is

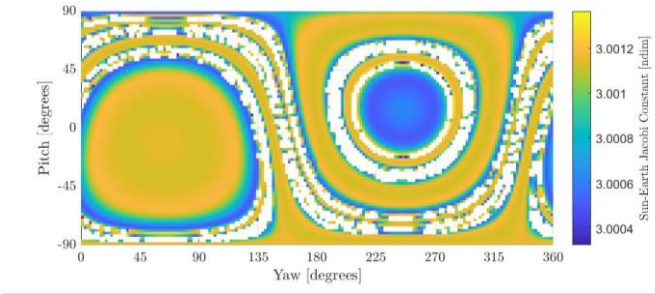

Figure 10: Sun-Earth Jacobi Constant map for a 1 m/s jettison at apolune

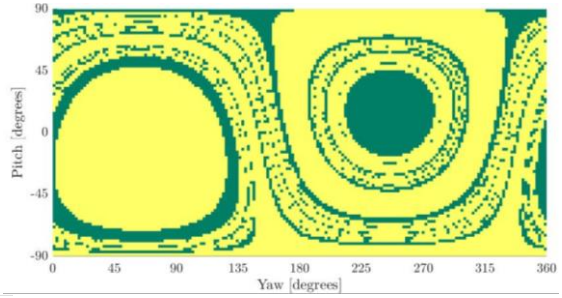

Figure 11: Energy departure map for a 1 m/s jettison at apolune. Green regions yield sufficient Jacobi Constant values for heliocentric escape

regenerated in Figure 11 to emphasize regions with sufficient energy to depart. The green regions mark maneuver directions in the VNB frame that achieve the desired Sun-Earth Jacobi Constant value. Conversely, yellow points mark the jettison directions resulting in trajectories with insufficient energy to pass through the L_1 or L_2 portals with a direct escape.

One challenge with identifying the trend in the Sun-Earth Jacobi Constant is the indirect relationship with Earth-Moon rotating states. Building intuition into the dynamics, and possible constraints, aids in the jettison design strategy. Consider a sample scenario where a jettisoned spacecraft is located in position space at the Earth-Moon L_2 point. The aim is to identify a velocity direction that maximizes the energy in the Sun-Earth rotating frame, which is equivalent to maximizing the Sun-Earth rotating velocity. The Sun-Earth rotating velocity vector is written as

$$\vec{v}_{SE} = \vec{r}_{EM}\dot{C} + \vec{v}_{EM}C$$

The terms $\vec{v}_{SE}$ and $\vec{v}_{EM}$ are the velocity vectors in the Sun-Earth and Earth-Moon rotating frames, respectively. The vector $\vec{r}_{EM}$ is the position vector of the object in the Earth-Moon rotating frame, relative to the Earth-Moon barycenter. The direction cosine matrix C maps states from one rotating frame to the other, and is written as

$$C = \begin{bmatrix} cos(\theta_S) & -sin(\theta_S) & 0 \\ sin(\theta_S) & cos(\theta_S) & 0 \\ 0 & 0 & 1 \end{bmatrix}$$

Recall the angle θ_S orients to the two rotating frames. The derivative of the rotation matrix ($\dot{C}$) is,

$$\dot{C} = n \begin{bmatrix} -\sin(\theta_S) & -\cos(\theta_S) & 0 \\ \cos(\theta_S) & -\sin(\theta_S) & 0 \\ 0 & 0 & 0 \end{bmatrix}$$

The variable n is the mean motion of the Sun-Earth system relative to the Earth-Moon rotating frame. Note that the matrix C is unitary while the derivative $\dot{C}$ is not. To maximize the Sun-Earth rotating velocity $\vec{v}_{SE}$, the sum of $\vec{r}_{EM}\dot{C}$ and $\vec{v}_{EM}C$ must also be maximized. The combination of two vectors is maximized when the vectors are aligned. Taking the dot product between $\vec{r}_{EM}\dot{C}$ and $\vec{v}_{EM}C$ yields,

$$n(-xsin(\theta_S) - y\cos(\theta_S)) * (\dot{x}\cos(\theta_S) - \dot{y}\sin(\theta_S)) + \cdots$$

$$n(xcos(\theta_S) - y\sin(\theta_S)) * (\dot{x}\sin(\theta_S) + \dot{y}\cos(\theta_S)) = n(x\dot{y} - y\dot{x})$$

$$h_z = (x\dot{y} - y\dot{x})$$

Note that the cartesian states are in the Earth-Moon rotating frame. The term h_z is the z-component of angular momentum of the object in the Earth-Moon rotating frame. The result illustrates that maximizing the Sun-Earth energy, i.e., reducing the Jacobi Constant value, is obtained by maximizing h_z. To illustrate the angular momentum term, a map for a 1 m/s jettison at apolune is constructed in Figure 12. The color scale indicates h_z of the trajectory at the departure state (450,000 km from the Earth), where yellow regions signify large values. The regions in white do not reach 450,000 km from Earth in the 90-day timeframe. Comparing Figure 10 to Figure 12 demonstrates the inverse relationship between the Sun-Earth Jacobi Constant value and h_z. One benefit to the connection between energy and angular momentum is the simplicity of targeting h_z in the Earth-Moon rotating frame. For a jettison maneuver with a fixed magnitude, targeting a value of $h_z > 0$ (prograde) at 450,000 km from Earth yields transfers that have the necessary Sun-Earth energy to escape through the L_1 and L_2 portals.

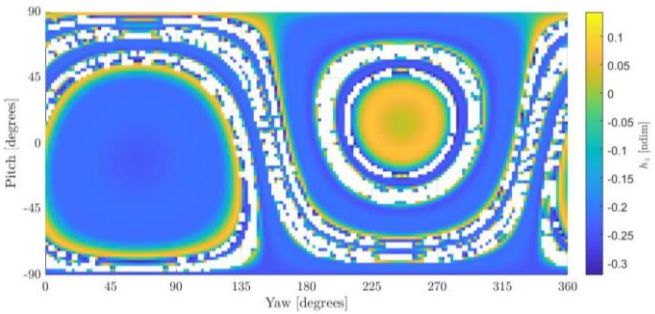

Figure 12: Earth-Moon angular momentum map for a 1 m/s jettison at apolune

Disposal strategies require suitable timing to escape to heliocentric space. One challenge is associated with connecting the jettison epoch with a sufficient phase of the Earth-Moon-Sun system. The process includes several components: initial epoch identification, time to depart, and orientation.

1 Initial epoch identification matches the selected location along the orbit with a given orientation of the Earth-Moon-Sun system. The CR3BP is time-independent, however, the introduction of the Sun with the BCR4BP creates a time-dependency. One condition that is leveraged is the synodic resonance of the 9:2 NRHO. Since the geometry is resonant with the Earth-Moon-Sun synodic period, jettison patterns repeat every two months. Although the patterns repeat, the phase of the NRHO is still required. The NRHO phase describes the alignment of the 9:2 structure with the Earth-Moon-Sun system. For Gateway, the NRHO is placed in a specific geometry for long-term eclipse avoidance.[18] The geometry places a perilune precisely when the Moon falls between the Sun and Earth, i.e., $\theta_S = 0^o$. For ease, the perilune at $\theta_{S,n}$ is defined as revolution n, where revolution one starts at $\theta_{S,1} = 0^o$. Since the Sun traverses clockwise relative to the Earth-Moon system, the remaining perilunes occurs every -80 degrees, i.e., revolution 2 starts at $\theta_{S,2} = -80^o$, revolution 3 starts at $\theta_{S,3} = -160^o$, etc. Likely a jettison occurs away from perilune, thus, the time past perilune (t_{pp}) multiplied by the angular rate yields the angle swept over that timeframe ($\theta_S(t_o) = \theta_{S,n} + \dot{\theta}_S\, t_{pp}$. For example, consider a jettison maneuver at apolune on the 5th revolution of the NRHO. The angle of perilune on the fifth revolution equates to $\theta_{S,5} = -80 * 5 = -400 = -40^o$. Apolune occurs at a time past perilune of 3.28 days, while the angular rate of the Sun about the Earth-Moon system is -12.19 degrees per day. Thus, the initial Sun angle for a jettison at apolune of revolution 5 is $\theta_S(t_o) = -40 - (12.19) * 3.28 = -80^o$. A way to validate this process is the dual resonance of the NRHO; a perilune for one month should equate to an apolune for the next. For example, the perilune of the second revolution has the same Earth-Moon-Sun orientation as the apolune on the fifth revolution.

2 The time to depart from the NRHO ties the initial jettison epoch with the relative phase of the Earth-Moon-Sun system at departure. Following the same procedure as the Jacobi Constant map, a grid of jettison directions is applied for a fixed location along the NRHO and a fixed jettison maneuver magnitude. The time it takes for each trajectory arc to reach 450,000 km is denoted the time to depart and given the symbol t_d. A time to depart map for the 1 m/s jettison at apolune sample scenario appears in Figure 13. The shortest time to depart in this example is 46 days. Recall the white areas of the map do not result in departures exterior to the Moon over the 90-day time horizon. The time to depart is coupled with the mean motion of the Sun to determine the evolution of the Earth-Moon-Sun geometry while the objects traverse through cislunar space. The change in Sun angle over the timeframe is computed using $\Delta\theta_S = \dot{\theta}_S\, t_d$. Take for example a transfer that requires 60 days to reach the departure condition. Recall, the angular rate of the Sun about the Earth-Moon system is -12.19 degrees per day. For a 60-day trajectory, the change in Sun angle is $\Delta\theta_S = -731.4^o$, or reduced to $\Delta\theta_S = -11.4^o$.

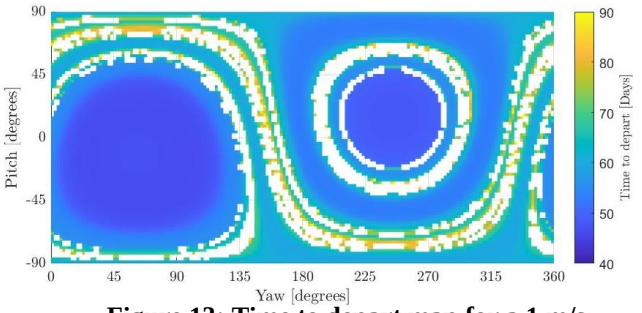

Figure 13: Time to depart map for a 1 m/s jettison at apolune

3 Heliocentric escape requires proper orientation to pass through the L_1 and L_2 portals. The relative location of the departure state in the Sun-Earth system dictates whether a trajectory performs a direct escape or completes additional revolutions within the Earth-Moon system. In the planar CR3BP, the stable and unstable manifold structures are separatrices for planar periodic orbits.[19] The L_1 and L_2 Lyapunov orbit manifolds bound motion between near-Earth and heliocentric space. To identify the proper disposal method, the stable manifold structures are explored. An assumption made to assess the bounding manifold flow is that the departing motion from the NRHO lies in the ecliptic plane. The L_1 and L_2 Lyapunov orbits are constructed for a Sun-Earth Jacobi Constant value of 3.0007. Recall the departure state is defined at the location 450,000 km from Earth. Trajectories along the stable manifolds of the two Lyapunov orbits are propagated in reverse time. A Poincaré section

of a circle with radius 450,000 km from Earth is employed. Each time a trajectory along the manifold passes through the section, the state is recorded. Polar coordinates centered at the Earth are employed to evaluate the manifold typology. The angle Γ measures the position of the state relative to the +*x*-axis in the Sun-Earth rotating frame, centered at Earth. The angle is termed the Moon angle, as it orients the approximate position of a departing object and the Moon within the Sun-Earth frame at a given epoch. An illustration of the typology is depicted in Figure 14. The blue and orange points correspond to the stable manifold crossings associated with the L_1 and L_2 Lyapunov orbits, respectively. Both orbits have a Sun-Earth Jacobi Constant value of 3.0007. The manifold structures bound passage to heliocentric space. Therefore, a point within the blue curves traverses out L_1 interior to the Sun-Earth system. Likewise, a departure state from the orange curve moves through the L_2 portal, exterior to the Sun-Earth system. Note that the sections evolve as the Sun-Earth Jacobi Constant value changes. In addition, the radial velocity is likely to change with each departure state. Therefore, the Poincaré section from Figure 14 acts as a reference, where a conservative estimate on escape states is selected. The orientation of the departure state is tied to the angle range for the Moon angle Γ. The escape sets selected are $\Gamma_{L_1} = [20^o, 135^o]$, and $\Gamma_{L_2} = [-160^o, -45^o]$.

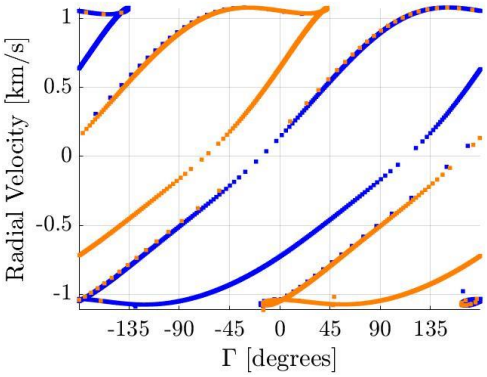

Figure 14: Poincaré section to assess heliocentric escape leveraging stable manifolds off the L_1 and L_2 Lyapunov orbits. (JC = 3.0007)

Insights from the initial epoch selection, time to depart, and orientation enable a strategy for direct heliocentric escape. The goal is to determine the position of the Sun relative to the Earth-Moon system when the jettisoned object reaches the departure state (450,000 km from Earth). The Sun angle at the departure state is strictly a function of the initial Sun angle and time to depart, i.e., $\theta_S(t_d + t_0) = \theta_S(t_0) + \dot{\theta}_S t_d$. Rotating the departure state from the Earth-Moon to the Sun-Earth rotating frame enables a comparison to the orientation analysis. The state is projected onto the ecliptic plane, and the Moon angle Γ is determined. If the Moon angle is in either escape sets Γ_{L_1} or Γ_{L_2}, then the departure orientation is sufficient for heliocentric escape. Return to the sample scenario of a 1 m/s jettison at apolune. Assume the jettison occurs on either revolution 1 or revolution 2 of the NRHO. The maps in Figure 15 illustrate jettison maneuver directions that predict escape through the L_1 or L_2 portals. The areas in blue signify transfers that have the proper orientation to depart through the L_1 portal, interior to the Sun-Earth system, while the orange regions predict jettison directions that yield orientations that may escape through the L_2 portal and traverse exterior to the Sun-Earth system. Revolution 1 and 2 are depicted by Figure 15a and Figure 15b, respectively. It is apparent that the orientation jettison options change from revolution to revolution. Note that the map does not include information about the energy at departure, therefore, Figure 15 does not predict escape. Although the immediate dynamics of the departure phase are not primarily governed by the Sun, once the object reaches the departure state, the relative orientation of the Sun has a large influence in the potential for heliocentric escape.

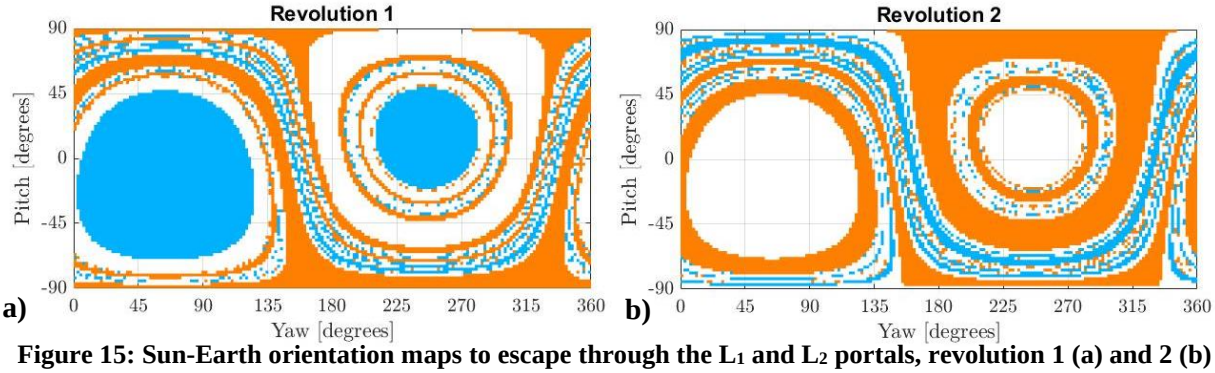

Figure 15: Sun-Earth orientation maps to escape through the L_1 and L_2 portals, revolution 1 (a) and 2 (b)

Jettison maneuver analysis is influenced by errors observed in operational flight. The applications complementing analysis of this analysis involves the introduction of maneuver execution errors and navigational errors from the initial jettison state.[20] The findings identify a desired jettison geometry that is less perturbed by errors. The geometry is denoted a 'corner turn'; an example is illustrated in Figure 1. A method to differentiate the geometry from other transfers is to assess if the departure state has a z-component greater than zero. The 3D maps in Figure 16 represent the maneuver directions (yaw and pitch) that yield corner turn departures for TA values from 0º to 360º around the NRHO. Three values of jettison Δv magnitude are represented, 1.7 m/s, 5 m/s, and 15/ m/s. Each point on the map represents a single jettison location and direction that results in a corner-turn departure from the NRHO. Since each point in Figure 16 represents a corner-turn departure, the points are colored according to the NRHO time to depart, measured in terms of revolutions in the NRHO. It is apparent that a larger maneuver generally leads to a faster departure. As observed in previous studies, the fastest departures are achieved by maneuvers in a lobe centered around the velocity direction (yaw = pitch = 0º) at perilune (TA = 0º). It is also notable that each lobe or shell within the 3D maps is comprised of a set of maneuvers that tend to depart after the same time-of-flight. These maps demonstrate that a given desired behavior is available at a range of locations along the NRHO if the maneuver direction or magnitude is varied. Similarly, the same behavior is available across various jettison Δv magnitudes if the direction and/or TA are adjusted. The behavior of trajectories departing the NRHO is cyclic in TA, Δv, and maneuver direction.

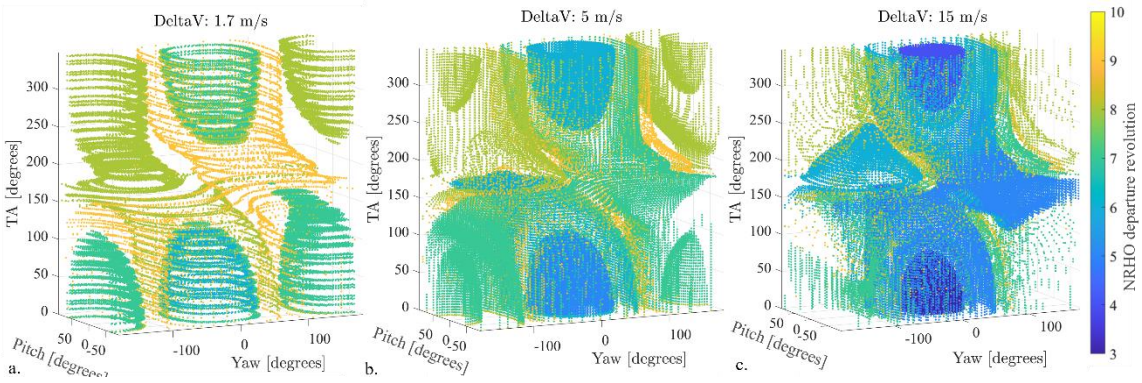

Figure 16: Maneuver directions that yield corner-turn departures for 1.7 m/s (a), 5 m/s (b), and 15 m/s (c) jettisons

Combining feasible jettison directions from the Sun-Earth Jacobi Constant map and the orientation map yields a strategy to identify direct heliocentric escapes. Sufficient energy and proper Sun-Earth departure orientation is required to escape to heliocentric space. Return to the sample scenario of a 1 m/s jettison maneuver at apolune along the NRHO. The Jacobi Constant map from Figure 17 illustrates jettison directions that yield sufficient energy to pass through the L_1 or L_2 portals. Likewise, the orientation maps included in Figure 17 signify jettison directions that result in the correct Sun-Earth orientations. Based on the revolution of the NRHO, Figure 17 illustrates heliocentric escape maps. Heliocentric escape maps are generated for the first four revolutions of the NRHO, labeled Figure 17a) through d), respectively. The green regions represent jettison maneuver directions that predict heliocentric escape. It is apparent that there are repeated trends from revolution to revolution.

JETTISON MAP

Jettison from NRHO requires careful selection of the maneuver from the baseline NRHO. Recall the first two phases of NRHO disposal are NRHO departure and heliocentric escape. Operational and dynamical constraints must be considered to avoid conjunctions and escape to heliocentric space. Overlaying recontact, range flip, heliocentric escape, and corner turn information onto one map offers a visual for selecting initial jettison directions. Assume the sample scenario case of a 1 m/s jettison at apolune (associated with revolution 1). The jettison map is illustrated in Figure 18. The title of the plot indicates the revolution of the maneuver and the Moon angle Γ at the time of jettison. The yaw and pitch are relative to an inertial VNB frame. The regions in red refer to jettison directions that result in a recontact, i.e., return within the keep-out-zone of 100

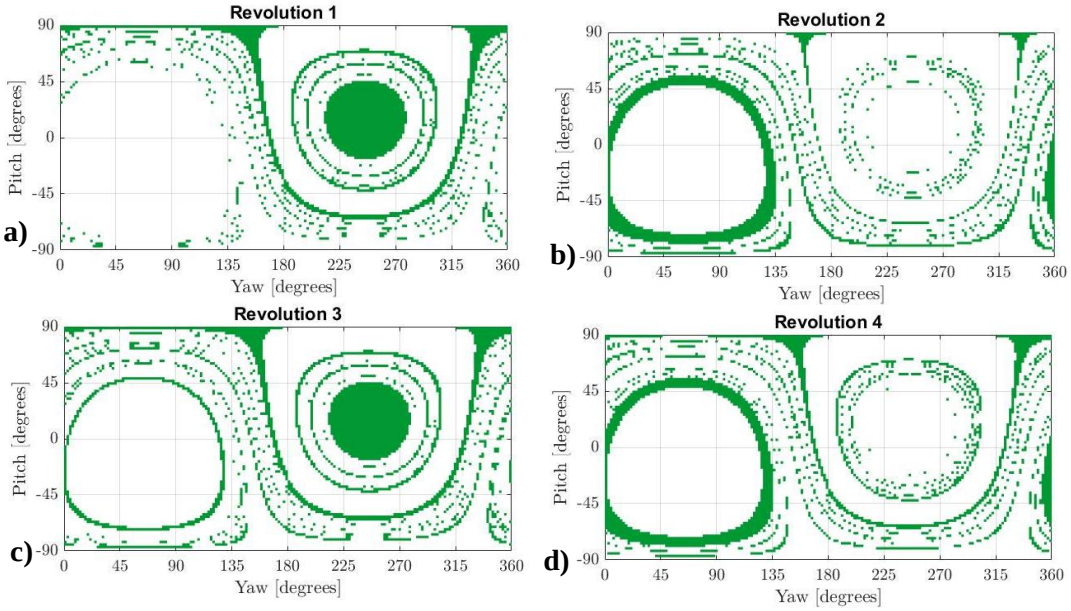

Figure 17: Heliocentric escape maps for 1 m/s jettison at apolune, revolution 1 (a), 2 (b), 3 (c), and 4 (d)

km. The areas marked by pink dots signify jettison directions that have a perilune range flip. The blue points result in disposal geometry that matches a desired corner turn behavior but does not guarantee the proper orientation. The green regions yield heliocentric escape. The aim is to select a jettison location (or regions) where the blue points overlap a green region, while avoiding the red and pink areas. It becomes apparent that heliocentric disposal without conjunction events it a nontrivial task to predict when treated as a single problem. However, separating each phase into different challenges reduces the complexity of the problem.

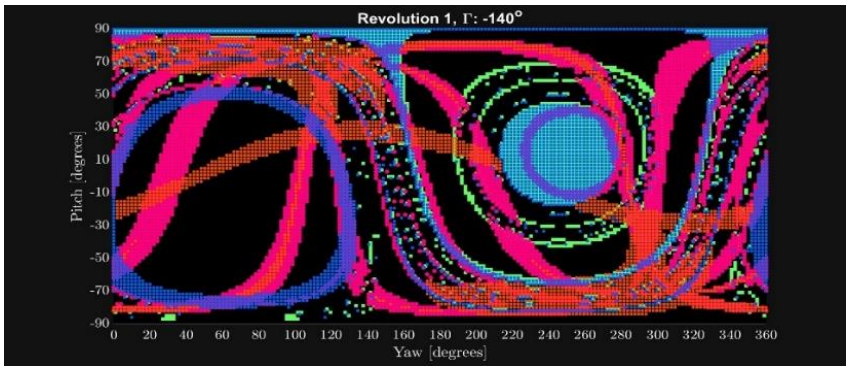

Figure 18: Jettison map for a 1 m/s maneuver at apolune (revolution 1 of the NRHO)

PROBABILITY OF CONJUNCTION

Identifying the probability of recontact and range flip offers insight into mission planning. Inadvertent jettisons could be the result of maneuver execution errors, an emergency abort, or miscellaneous debris from cislunar operations. Due to the dimensionality of the problem, a similar mapping technique is employed at different locations along the NRHO. Assume debris is inadvertently jettisoned from Gateway with a maneuver magnitude of 1 m/s. The maps from Figure 7 and Figure 9 provide an illustration for possible jettison directions. Without knowledge of the maneuver direction, it is uncertain if a recontact or flip will occur. Rather than constructing a map using the grid technique, a Fibonacci spiral with 5000 points is employed.

The technique aims to maintain equal spacing in every direction. As an inadvertent jettison may occur at any time, maps are generated at different locations along the orbit. A set of recontact maps and flip maps are combined to create 3D maps, illustrated in Figure 19a and Figure 19b, respectively. Each blue point corresponds to a maneuver direction and NRHO location that results in a recontact (Figure 19a) or flip (Figure 19b). The recontact and range flip distances remain at the set 100 km and 1000 km values, respectively. The jettison maneuver magnitude remains 1 m/s. A horizontal cross-section of Figure 19a or Figure 19b yields a map at a fixed location on the NRHO. The vertical axis is the location on the NRHO defined by time past perilune. Note that the surface geometry evolves as the time past perilune changes, thus, the jettison location greatly impacts the proability of recontact or a flip. The probability of conjunction is determined by dividing the number of conjunction events by the total number of points for each location along the NRHO. For example, out of the 5000 points selected at perilune, 129 of them result in a recontact within the set 100 km range. Thus, the probability of recontact for an inadvertent jettison of 1 m/s, at perilune, is 2.58%.

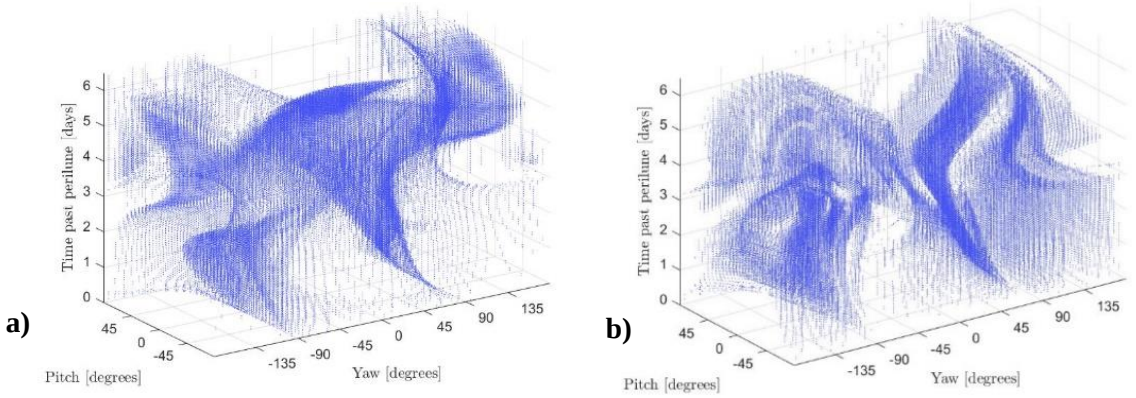

Figure 19: Three-dimensional recontact (a) and flip (b) map for a 1 m/s jettison along the NRHO

The favorability for jettison of a given TA along the NRHO can be assessed in part by computing the percentage of total jettison directions at that location that yield desirable or undesirable behavior. Three quantities of interest in this study are independent of Sun angle: undesirable jettisons result in recontact risk or range flips at perilune; desirable jettisons result in corner-turn departures (whether those departures then continue to directly escape to heliocentric space depends on the Sun angle.) The percentage of total maneuvers that yield corner turn departures, perilune range flips, and recontact risk appear as a function of jettison TA in Figure 20 for 1.7 m/s, 5 m/s, and 15 m/s maneuvers as computed in the CR3BP. Each datapoint represents the results of 5,000 maneuver directions equally distributed in a sphere using a Fibonacci spiral distribution applied at a single jettison TA. For each TA, the percentage of the 5000 jettison directions that yield corner-turn departures is plotted in blue, the percentage that results in a trajectory that re-enters the 100 km keep-out sphere is plotted in red, and the percentage of total maneuver directions that experience a perilune flip in the range resulting in an approach within 1000 km of the Gateway is plotted in magenta. Note that these results are not exclusive; it is possible for a single jettison trajectory to experience a recontact risk shortly after jettison, a flip in the range pattern at perilune several revolutions later, and a corner-turn departure. It is also possible for a jettison trajectory to experience none of these metrics. Several notable observations are apparent in . First, for each jettison Δv magnitude, certain locations along the NRHO are associated with a maximum number of outcomes of each type. For example, for Δv = 1.7 m/s, the percentage of maneuver directions yielding corner-turn departures reaches nearly 30% at TA = 110º. However, jettison locations within 120º of perilune are avoided due to high sensitivity, challenging attitude dynamics, and poor state knowledge in the vicinity of perilune, so this jettison location is not suitable. If the jettison magnitude is increased to 5 m/s, a peak appears in the plot near apolune, such that 22% of jettison directions yield corner-turn departures at TA = 178º. Similarly, for Δv = 15 m/s, 25% of jettison directions result in corner-turn departures at TA = 155º. Selecting a jettison magnitude and location combination with a larger percentage of corner-turn outcomes yields jettison maps with larger swaths of blue, increasing the likelihood of robust jettison options when applied in a higher-fidelity ephemeris model. In simple terms, it is easier to find a good solution when more directions give desirable outcomes. Similarly, avoiding jettison locations that yield a

larger percentage of cases resulting in recontact risk or perilune flips in the range increases the odds of a favorable departure.

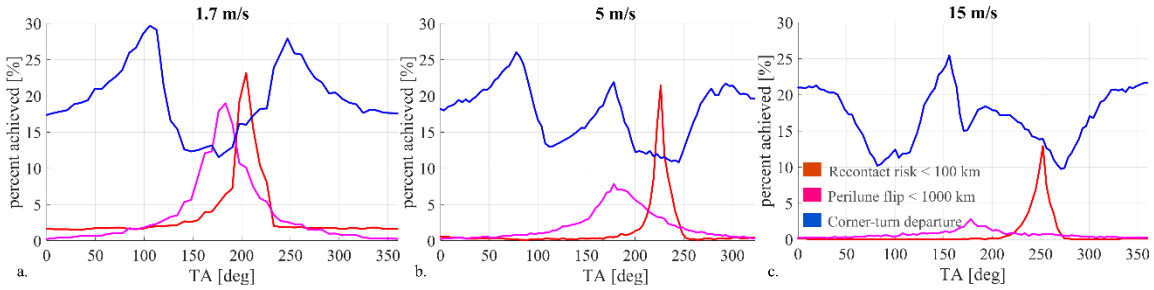

Figure 20: Percent of total jettison maneuver directions that result in recontact risk, perilune flips, and corner-turn departures for 1.7 m/s (a), 5 m/s (b), and 15 m/s (c) jettisons as a function of TA

Varying the jettison maneuver magnitude extends the probability curves to a surface. The process required to generate the curves from Figure 20 includes the construction of recontact and flip maps at fifty locations along the NRHO. Each map includes 5000 points to estimate the probability of each event, such that a total of 250,000 propagations are executed to describe the probability of conjunction events for a 1 m/s jettison maneuver magnitude. The process is repeated for 2 m/s to 15 m/s, at an interval of 1 m/s. The three-dimensional probability surfaces are illustrated in Figure 21. The surface in Figure 21a depicts the percent of jettison maneuver directions that result in a recontact within 100 km. The surface in Figure 21b illustrates the percent of jettison directions that have a range flip. The surfaces demonstrate how the percent achieved evolves as the jettison maneuver magnitude and location along the NRHO varies. For both Figure 21a and Figure 21b, blue represents a lower risk, while yellow is the higher risk. One observation between the two surfaces is that as the jettison maneuver increases, the probability decreases. From Figure 21a, the most likely location on the NRHO for a recontact arises when the jettison occurs just prior to perilune passage. It is apparent that a higher probability of a range flip exists for jettisons near apolune.

EARTH EVASION

The first two phases of the NRHO disposal strategy focus on the risk-mitigation and transfer design from cislunar space to orbiting the Sun. The resultant motion in heliocentric space is predominately governed by the Sun, with occasional passes of the Earth. The goal is to evade the Earth or maximize the closest approach to Earth over 100 years. Assume the motion of the object can be approximated as planar relative to the ecliptic plane. Lyapunov manifolds from the Sun-Earth CR3BP aid in the identification of assessable dynamical structures in this regime. Recall the heliocentric escape analysis in which transit flow is identified by passage through the manifold. For a planar transfer, any jettison that successfully reaches heliocentric space must be within the manifold tube corresponding to the Lyapunov orbit associated with the Jacobi constant of the post-

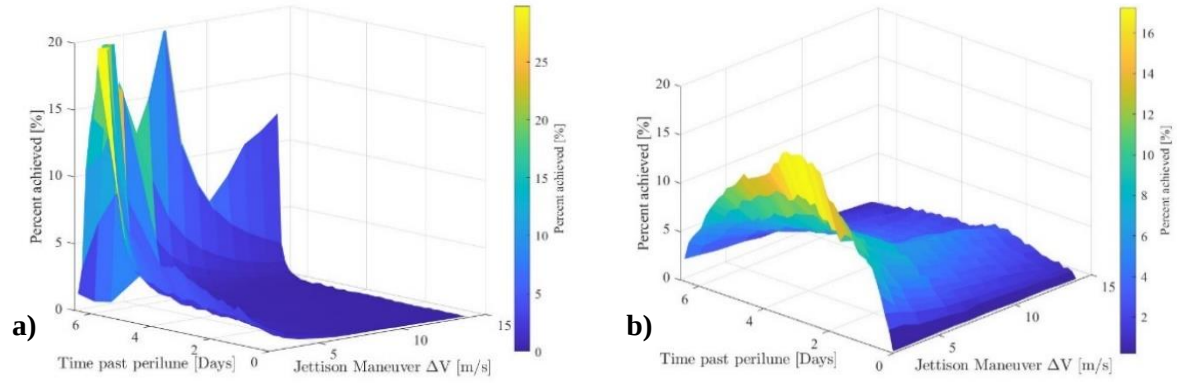

Figure 21: Evolution of conjunction events across the jettison location and maneuver magnitude: a) recontact map, b) perilune flip map

jettison trajectory. The challenge exists in predicting the evolution of the motion over time. Two metrics are considered to assess the viability of close approach to Earth: the osculating orbital period (T) and the argument of perihelion (ω). The osculating orbital period is computed assuming Keplerian motion of the object about the Sun. The argument of perihelion is measured relative to the Sun-Earth rotating frame, a schematic of the angle is depicted in Figure 22. The graphic marks a perihelion as the black circle. The angle is centered at the Sun and measured counterclockwise from the +x-axis of the Sun-Earth rotating frame. Consider an L_2 Lyapunov orbit with a Jacobi Constant value of 3.00065. Trajectories from the unstable and stable manifold arcs that depart near-Earth space are propagated to complete one full revolution about the Sun-Earth system. The osculating orbital period and argument of perihelion for the manifold structures is displayed in Figure 23. The blue and red points correspond to the stable and unstable manifold arcs, respectively. Note that a disposal trajectory is bounded by the red dots. As the stable manifold yields transfers that return close to the Earth, the intersections of the red and blue curves should be avoided. The propagation time for these transfers ranges from 10 to 20 years. To avoid the Earth for a longer time horizon, longer propagation is required. A set of 3000 points along the unstable manifold are selected. Each point is propagated for 100 years. The perihelion map in Figure 24 illustrates the results of the propagation. The color scale measures the close approach distance, where cyan points represent the closest approaches and magenta the furthest passages of the Earth. The magenta points represent the maximum close approach distances that are achievable from a jettison at the given value of Jacobi Constant. Part 2 of the current analysis[20] explores methods to achieve similar trajectories from NRHO jettisons. It becomes apparent that locations on the map where the stable and unstable manifold arcs intersect in Figure 23 corresponds to regions of light blue that are closer Earth passes in Figure 24.

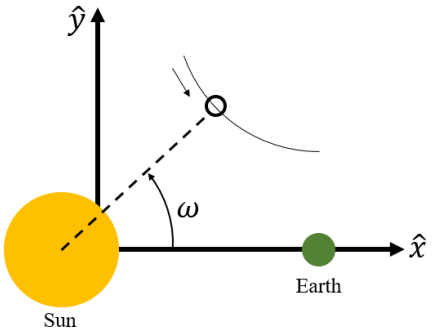

Figure 22: Schematic illustrating the argument of perihelion measured relative to the Sun-Earth rotating frame

The Poincaré section in Figure 24 illustrates inaccessible regions over a long-time horizon. This Poincaré map is a modification to previously explored Keplerian maps.[21] Ross and Scheeres explore similar structures in the vicinity of planet-moon systems, where the regions void of points are denoted stable islands.[22] The stable resonant orbit for an island is determined from the resonance ratio. A resonant orbit is given the nomenclature of p:q resonance, where the object completes p revolutions for every q revolutions completed by the system. For example, the 9:2 resonance of the NRHO refers to 9 periods of the orbit for every two synodic months. As the orbital period is close to 1 year, the resonances are n+1:n, where the value for n is computed by $n = \frac{1}{P-1}$. For an object with an osculating heliocentric period of P = 1.0769 years, the resonance ratio is determined to be 14:13. Constructing the corresponding resonant orbit in the CR3BP does not require a precise period, rather, the two-body approximation is employed as an initial guess. Leveraging a perpendicular crossing targeting scheme, the planar 14:13 resonance has three members with a Sun-Earth Jacobi Constant value of approximately 3.00065. Figure 25 illustrates the perihelion locations for the periodic resonant orbits

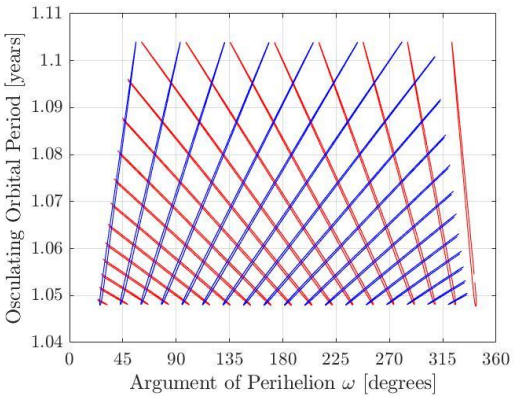

Figure 23: First Earth-return stable and unstable manifold perihelion Poincaré map (JC = 3.00065)

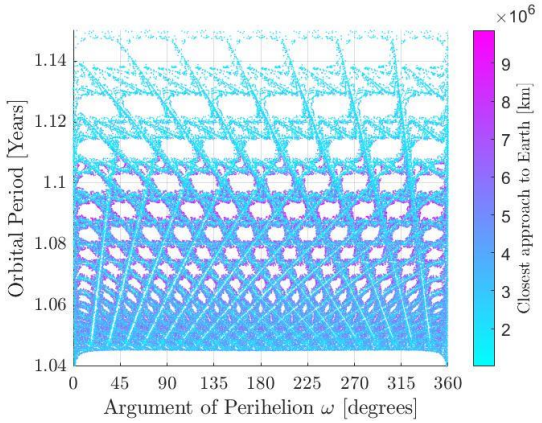

Figure 24: Perihelion Poincaré map constructed from 100-year unstable manifold propagation (JC = 3.00065)

relative to the constructed Poincaré map. The perihelion locations for the two unstable 14:13 resonant orbits are marked by black and red dots, while the stable orbit is indicated with black asterisks. Focusing in on the region around the stable period resonant orbit, solutions nearby on the map have larger close approach distances from Earth. The three periodic orbits are depicted in Figure 26a and Figure 26b, centered at the Sun and Earth, respectively. The solid black and red curves correspond to the unstable black and red points in Figure 25. Whereas the dotted black curve is the stable resonant orbit that is associated with the asterisk in Figure 25. The unstable structure is governed by the close passes of the Earth on each period of the orbit, whereas the stable solution passes through aphelion during the close approach, making the structure more robust to each Earth pass. From Figure 26a, it is apparent that the unstable and stable resonances have offset argument of periapsides. These structures offer insight into flow that departs from and arrives at Earth. Aiming to achieve the stable resonant orbit is infeasible along a ballistic curve. However, options exist about the stable solution that could lead to long-term Earth evasion. Accessing the stable island regions is explored utilizing quasi-periodic orbits. The stable 14:13 resonant orbit has a planar center subspace. A family of quasi-periodic orbits with a fixed Jacobi Constant is constructed. A state along the quasi-periodic orbit is propagated for 200 years and illustrated in Figure 27. The trajectory is depicted in the Sun-Earth rotating frame, centered at the Earth. Along each surface a set of trajectories is selected to assess the close approach distance from the Earth. Comparing Figure 27 to Figure 10 from part 2 of this analysis demonstrates that the long-term Earth evasion geometry persists in a higher fidelity ephemeris force mode.[20] However, as the family of quasi-periodic orbits remains linearly stable, the unstable manifold does not approach the same region. To illustrate this behavior, the corresponding perihelion Poincaré map that includes the quasi-periodic orbits families is displayed in Figure 28. The concentric magenta dots correspond to different quasi-periodic orbits, filling the stable island. The surrounding sea of perihelia originate from the L_2 unstable Lyapunov orbit, propagated for 100 years (as in Figure 25). The quasi-periodic orbit with the closest approach remains more than 10 million kilometers away from Earth, while the trajectories originating from the unstable manifold yield close approach distances less than 10 million kilometers. It is apparent that the dark blue to purple points begin to approach the structure generated by the stable resonant and quasi-periodic orbits. The perihelion Poincaré sections aid in characterizing long-term Earth structures. Acquiring these structures from cislunar jettison is nontrivial. Part 2 of this analysis explores a strategy of targeting the osculating orbital period after heliocentric escape.[20]

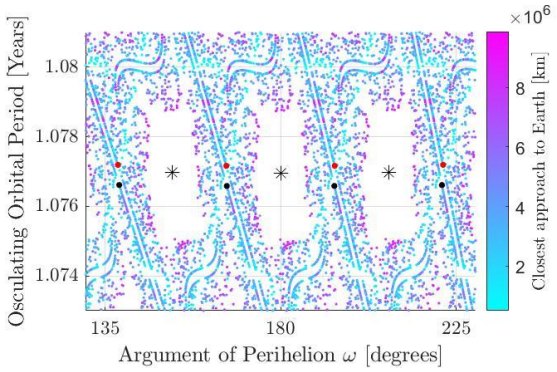

Figure 25 Perihelion Poincaré map with 14:13 resonance orbits in the Sun-Earth CR3BP (JC = 3.00065)

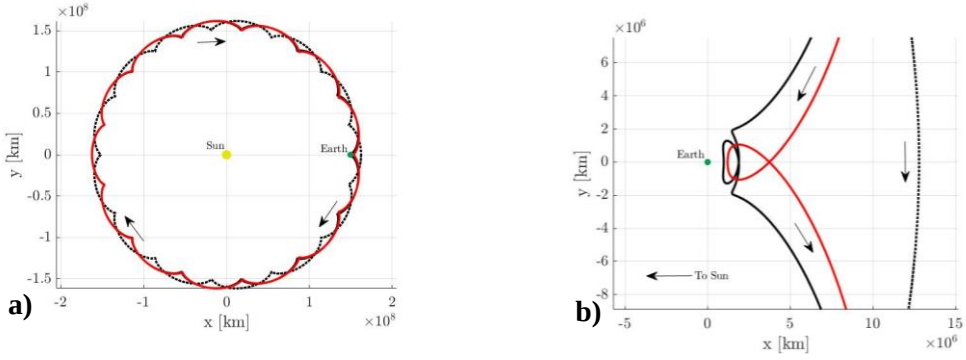

Figure 26: 14:13 resonant orbits in the Sun-Earth rotating frame, a) centered at the Sun, b) centered at Earth (JC = 3.00065)

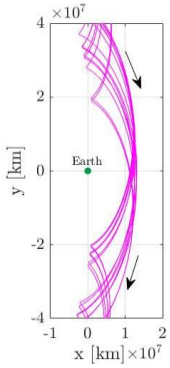

Figure 27 Trajectory off a quasi-periodic orbit, propagated for 200 years (Sun-Earth rotating frame)

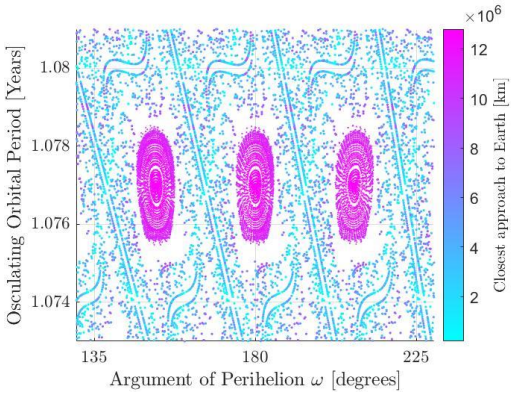

Figure 28: Perihelion Poincaré map with quasi-periodic orbit family in the Sun-Earth CR3BP

CONCLUDING REMARKS

Disposal and jettison techniques from cislunar space are feasible with proper timing and operations. Key challenges arise in connecting transfer structures across varying dynamical regimes. The current investigation brings together several phases of NRHO disposal strategies into one end-to-end process. The NRHO departure phase addresses the immediate concern of conjunctions during NRHO departure. Methods of constructing recontact maps and flip maps provide a detailed look into jettison options for a specific location along the NRHO. Exploring properties of the recontact maps provides additional information regarding the conjunction events, including relative velocity, location along the NRHO, and the number of recontacts. After departing the NRHO, a jettisoned object encounters the next challenge of heliocentric escape. Simplifying assumptions regarding the jettisoned trajectory aid in the identification of departure structures that traverse from the Earth-Moon to the Sun-Earth system. With adequate energy and timing, a ballistic arc from the NRHO carries the object to orbit around the Sun. The Sun-Earth Jacobi Constant value is employed as an energy metric to assess the validity of traversing through the L_1 and L_2 portals. The construction of Jacobi Constant maps provides jettison directions that offer sufficient energy to escape. A relationship between the Earth-Moon angular momentum and the Sun-Earth Jacobi Constant allows a targeting strategy that is independent of epoch and remains in the Earth-Moon rotating frame. Heliocentric escape also relies on proper orientation of the Earth-Moon-Sun system. Leveraging stable manifolds from the L_1 and L_2 Sun-Earth Lyapunov orbits yields accessible regions to heliocentric space. The combination of NRHO departure and heliocentric escape offers mission designers a map to traverse safely and efficiently through cislunar and heliocentric space. An inadvertent jettison analysis explores the probability of returning within the keep-out-zone, experiencing a perilune range flip, or reaching a corner turn geometry. The probabilities are assessed at varying locations along the orbit and for different jettison maneuver magnitudes. Risk assessment is crucial to mission operations. Once the object has escaped to heliocentric space, exploring behaviors in the Sun-Earth CR3BP offers insight into accessible structures. Unstable manifold structures from the L_2 Lyapunov orbit highlights accessible paths to departing flow. Leveraging a perihelion Poincaré mapping technique uncover islands void of intersections. The region is associated with stable, resonant periodic orbits in the Sun-Earth CR3BP. Computing both the stable and unstable 14:13 resonant orbits for a given Jacobi Constant value illustrates the differences in Earth passage for long-term Earth evasion. The center subspace of the stable resonant orbit is extended to a family of fixed-Jacobi Constant quasi-periodic orbits. The periapsides from the quasi-periodic orbits match the resonant islands and differentiate the stable orbits from the sea of unstable manifold crossing. Together the three phases of NRHO departure, heliocentric escape, and Earth evasion aim to provide a foundation to cislunar jettison and disposal analysis, recognizing that debris mitigation is feasible with limited propellant and operational capabilities.

ACKNOWLEDGEMENTS

The authors would like to thank Randy Eckman and Dale Williams for insightful discussions. The authors also recognize extensive previous contributions by Kenza Boudad that laid the groundwork for the analysis in this paper.

REFERENCES

[1] Olikara, Z. P., Gomez, G., and Masdemont, J. J., "End-of-life disposal of libration point orbit spacecraft". *64th International Astronautical Conference*. Beijing, China, 2013, IAC-13.C1.8.6

[2] Colombo C., Letizia F., Soldini S., Lewis H., Alessi E. M., Rossi A., Vasile M., Vetrisano M., and Van der Weg W., "End-Of-Life Disposal Concepts for Lagrange-Point and Highly Elliptical Orbit Missions", Final Report, ESA/ESOC contract No. 4000107624/13/F/MOS, Version 2.0 – 10 February 2014.

[3] R. Whitley and R. Martinez, "Options for Staging Orbits in Cis-Lunar Space," IEEE Aerospace 2015, March 2015.

[4] Williams, J., Lee, D. L., Whitley, R. J., Bokelmann, K. A., Davis, D. C., and Berry, C. F., "Targeting Cislunar Near Rectilinear Halo Orbits for Human Space Exploration". *AAS/AIAA Space Flight Mechanics Meeting.* San Antonio, Texas, 2017

[5] Guzzetti, D., Zimovan, E., Howell, K., and Davis, D. "Stationkeeping Analysis for Spacecraft in Lunar Near Rectilinear Halo Orbits". *27th AAS/AIAA Space Flight Mechanics Meeting.* San Antonio, Texas, 2017

[6] Boudad, K., Davis, D., and Howell, K. "Disposal Trajectories from Near Recitilinear Halo Orbits". *AAS/AIAA Astrodynamics Specialists Conference.* Snowbird, Utah, 2018

[7] Davis, D., Boudad, K., Phillips, S. and Howell, K. "Disposal, Deployment, and Debris in Near Rectilinear Halo Orbits". *29th AAS/AIAA Space Flight Mechanics Meeting.* Ka'anapali Maui, Hawaii, 2019

[8] Phillips, S. M., Davis, D. C., and Sweeney, D. J. "Cloud Computing Methods for Near Rectilinear Halo Orbit Trajectory Design" *AAS/AIAA Astrodynamics Specialists Conference,* Portland, ME, 2019

[9] Davis, D., Boudad, K. K., Power, R. J., and Howell, K. C. "Heliocentric Escape and Lunar Impact From Near Rectilinear Halo Orbits". *AAS/AIAA Astrodynamics Specialists Conference,* Portland, Maine, 2019

[10] Guardabasso, P., Lizy-Destrez, S., and Ansart, M. "Lunar Orbital Debris Mitigation: Characterisation of the Environment and Identification of Disposal Strategies". *8th European Conference on Space Debris (Virtual),* 2021

[11] Davis, D., Power, R., Howell, K., and Gutkowski, J. "Lunar Impact Probability for Spacecraft in Near Rectilinear Halo Orbits". *31st AAS/AIAA Space Flight Mechanics Meeting,* Charlotte, North Carolina, 2021

[12] Davis, D. C., Zimovan-Spreen, E. M., Power, R.J., and Howell, K. C. "Cubesat Deployment from a Near Rectilinear Halo Orbit". *AIAA SciTech Forum,* San Diego, California, 2022

[13] B. D. Anderson, M. W. Lo, and M. Vaquero. "The stability of orbital resonances for Europa quarantine design: escape orbit case." *AAS/AIAA Space Flight Mechanics Meeting*, Ka'anapali, Maui, Paper AAS 19-481, 2019.

[14] Zimovan-Spreen, E., Davis, D., and Howell, K. "Recovery Trajectories for Inadvertent Departures from an NRHO". *31st AAS/AIAA Space Flight Mechanics Meeting,* Charlotte, North Carolina, 2021

[15] Scheuerle, S.T., McCarthy, B. P., and Howell, K.C., "Construction of Ballistic Lunar Transfers Leveraging Dynamical Systems Techniques," *AAS/AIAA Astrodynamics Specialists Conference,* Lake Tahoe, California (Virtual), 2020

[16] Szebehely, V. *Theory of Orbits: The Restricted Problem of Three Bodies.* Academic Press, New York, 1967

[17] Hardin, D. P., Michaels T. J., and Saff E. B. "A Comparison of Popular Point Configuration of S^2," October 24, 2016

[18] Zimovan-Spreen, E. M., S.T. Scheuerle, B. P. McCarthy, D. C. Davis, and K. C. Howell, "Baseline Orbit Generation for Near Rectilinear Halo Orbits," AAS/AIAA Astrodynamics Specialists Conference, Big Sky, Montana, August 2023.

[19] C. Conley. "Low energy transit orbits in the restricted three-body problem". SIAM Rev. Soc. ind. Appl. Math, 16:732–746, 1968.

[20] Davis, D. C., Scheuerle, S. T., McCarty, S. L., Zimovan-Spreen, E. M., McCarthy, B. P., McGuire, M. L., and Howell, K. C. "Jettison and Disposal from Near Rectilinear Halo Orbits, Part 2: Applications," *AAS/AIAA Astrodynamics Specialists Conference*, Big Sky, Montana, 2023

[21] T. Y. Petrosky and R. Brouke, Area-preserving mappings and deterministic chaos for nearly parabolic motions, Celestial Mechanics, (1988), pp. 53–79.

[22] Ross, Shane & Scheeres, D.. (2007). Multiple Gravity Assists, Capture, and Escape in the Restricted Three-Body Problem. SIAM Journal on Applied Dynamical Systems. 6. 576-596. 10.1137/060663374.